FTs and out-of-equilibrium experiments

Alberto Imparato

Dipartimento di Fisica, Università di Trieste
Italy

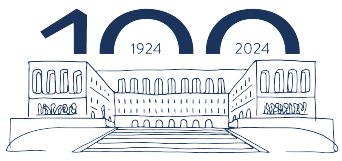

Dipartimento di
Fisica
Dipartimento d'Eccellenza 2023-2027

Fluctuation Relations

- Probability of the reversed path

$$\widehat{\mathcal{P}}[\widehat{\boldsymbol{x}} \mid \widehat{x}(0)] = \mathcal{P}[\boldsymbol{x} \mid x(0)]\, \mathrm{e}^{-\beta \mathcal{Q}^{\mathrm{B}}[\boldsymbol{x}]}$$

- Unconditional probabilities: Crooks' relation

$$\widehat{\mathcal{P}}[\widehat{\boldsymbol{x}}] = \mathcal{P}[\boldsymbol{x}]\, \mathrm{e}^{-\beta(\mathcal{W}[\boldsymbol{x}] - \Delta F)}$$

- Integral fluctuation relation: Jarzynski's equality

$$\left\langle \mathrm{e}^{-\beta \mathcal{W}} \right\rangle = \mathrm{e}^{-\beta\, \Delta F}, \qquad \text{with } Z_{\lambda(0)} / Z_{\lambda(t_f)} = \exp(\beta\, \Delta F)$$

- Detailed fluctuation relation (aka Gallavotti-Cohen relation)

$$\widehat{\mathcal{P}}[\widehat{\boldsymbol{x}}] = \mathcal{P}[\boldsymbol{x}] \mathrm{e}^{-\Delta \mathcal{S}^{\mathrm{tot}}[\boldsymbol{x}]/k_B}, \qquad \text{with } \Delta \mathcal{S}^{\mathrm{tot}} = \Delta \mathcal{S}^{\mathrm{B}} + \Delta S^{\mathrm{sys}}$$

$$\mathcal{S}^{\mathrm{B}}[\boldsymbol{x}] = \textstyle\sum_\alpha \mathcal{Q}^{\mathrm{B}\alpha}[\boldsymbol{x}]/T_\alpha,\ \Delta S^{\mathrm{sys}} = k_B \log\left[p(x(0), t_0)/p(x(t_f), t_f)\right]$$

Are they useful?

- Mechanical unfolding of biopolymers (Nucleic Acids, Proteins)

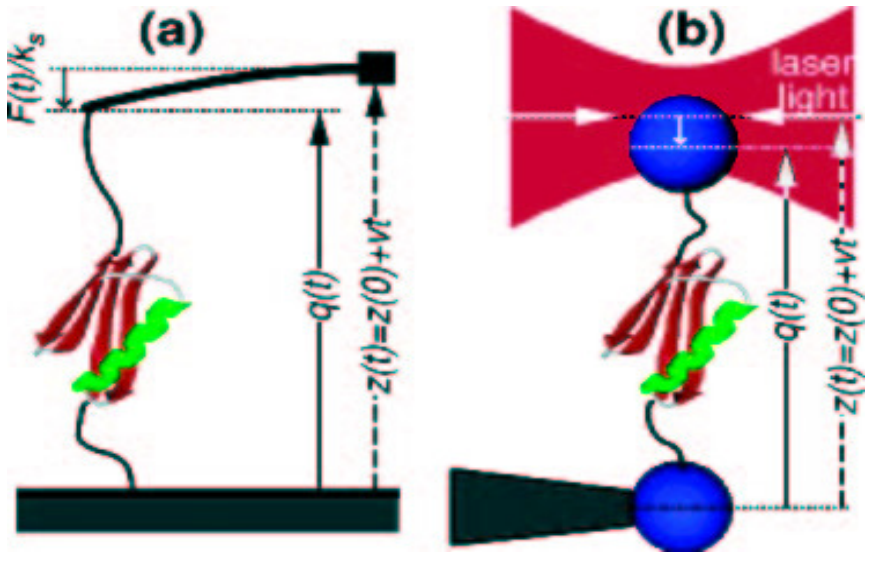

- Experiments performed in non-reversible conditions
- Out-of-equilibrium statistical mechanics can be used to evaluate equilibrium properties of the molecules

A Rna hairpin

$$\widehat{P}(-W) = P(W)\mathrm{e}^{-\beta(W-\Delta F)}; \qquad \widehat{P}(-W^*) = P(W^*) \Rightarrow W^* = \Delta F$$

D. Collin et al, Nature 2005

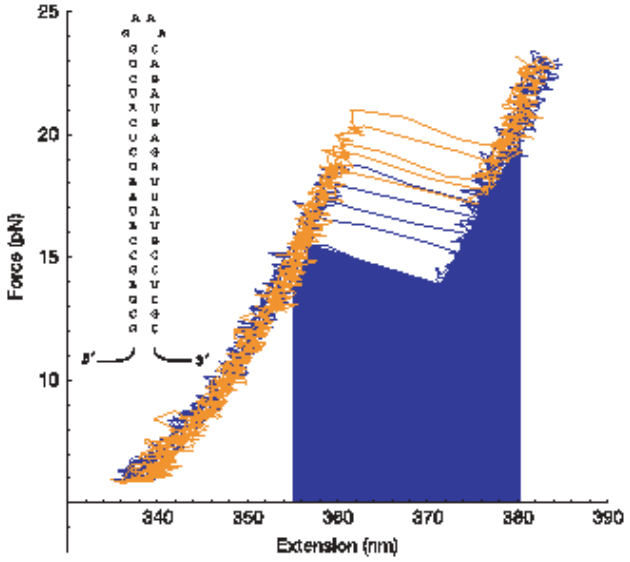

Figure 1 | Force–extension curves. The stochasticity of the unfolding and refolding process is characterized by a distribution of unfolding or refolding work trajectories. Five unfolding (orange) and refolding (blue) force–extension curves for the RNA hairpin are shown (loading rate of 7.5 pN s^{-1}). The blue area under the curve represents the work returned to the machine as the molecule switches from the unfolded to the folded state. The RNA sequence is shown as an inset.

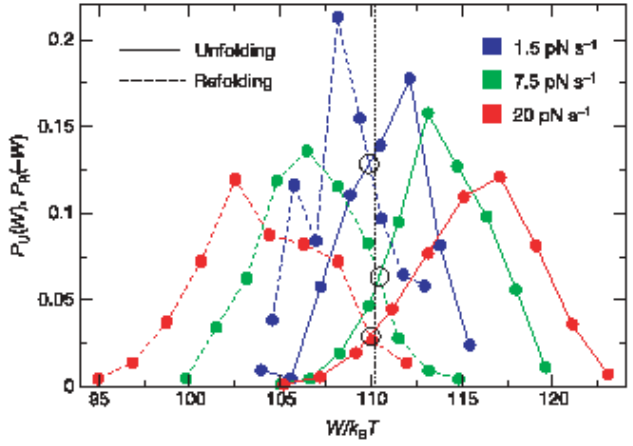

Figure 2 | Test of the CFT using an RNA hairpin. Work distributions for RNA unfolding (continuous lines) and refolding (dashed lines). We plot negative work, $P_R(-W)$, for refolding. Statistics: 130 pulls and three molecules ($r = 1.5\,\mathrm{pN\,s^{-1}}$), 380 pulls and four molecules ($r = 7.5\,\mathrm{pN\,s^{-1}}$), 700 pulls and three molecules ($r = 20.0\,\mathrm{pN\,s^{-1}}$), for a total of ten separate experiments. Good reproducibility was obtained among molecules (see Supplementary Fig. S2). Work values were binned into about ten equally spaced intervals. Unfolding and refolding distributions at different speeds show a common crossing around $\Delta G = 110.3\,k_BT$.

System in a steady state

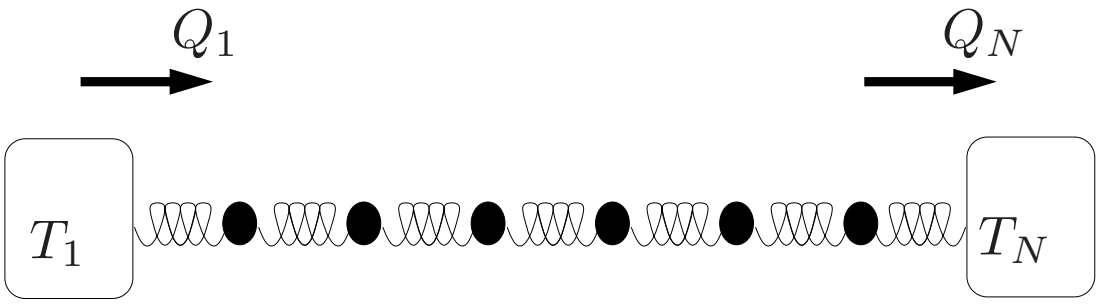

- $H = \sum_{i=1}^{N} \frac{p_i^2}{2m} + \frac{K}{2}\left[q_1^2 + q_N^2 + \sum_{i=1}^{N}(q_{i+1} - q_i)^2\right]$
- At equilibrium $T_1 = T_N$
  $\langle p_i p_j \rangle = 0$ if $i \neq j$
  $\langle q_i p_j \rangle = 0$, $\forall i, j$
- when $T_1 \neq T_N$ these variables are correlated
  Let $x = (q_1, \ldots q_N, p_1, \ldots p_N)$, and $C_{ij} = \langle x_i x_j \rangle$
  $P(x) = \exp\left[-\frac{1}{2} C_{ij}^{-1} x_i x_j\right] / \left[(2\pi)^N \sqrt{\det\left(C^{-1}\right)}\right]$
  Rieder, Lebowitz, Lieb, J. Math. Phys. (1967)

at exchanged by the i-th particle: Q_i

Langevin equations of motion

$$\begin{aligned}\frac{dq_i}{dt} &= \frac{\partial H}{\partial p_i} = p_i, \\ \frac{dp_i}{dt} &= -\frac{\partial H}{\partial q_i} + (-\Gamma p_i + \eta_i)\,(\delta_{1,i} + \delta_{N,i})\end{aligned}$$

Q_1 is our *macroscopic* observable

- $$Q_i = \int_{t_0}^{\Delta t} \mathrm{d}q_i \frac{\partial H}{\partial q_i} + \mathrm{d}p_i \frac{\partial H}{\partial p_i} = \int_{t_0}^{\Delta t} \mathrm{d}t p_i(t)\,(-\Gamma p_i + \eta_i)\,(\delta_{1,i} + \delta_{N,i})$$
- with Q_1 and $Q_N \neq 0$, and $Q_i = 0$, $i = 2, \ldots N-1$

Probability distribution $P(Q_1, t)$

- Exact result:
  $\sum_i Q_i = H(\{q_i(\Delta t)\}, \{p_i(\Delta t)\}) - H(\{q_i(t_0)\}, \{p_i(t_0)\})$
- One expects
  - $\langle Q_1 \rangle / t \propto (T_1 - T_N)$ in the long time limit
  - $\langle Q_1 \rangle = - \langle Q_N \rangle$

One can prove that, for any interaction potential and for $t \to \infty$

$$\boxed{P(Q_1) = P(-Q_1) \mathrm{e}^{-Q_1/\tilde{T}}},$$

where $k_B = 1$, and $\tilde{T} \equiv (1/T_1 - 1/T_N)^{-1}$
This is a particular case of a more general relation, the Gallavotti-Cohen relation

Simulations vs. exact solution

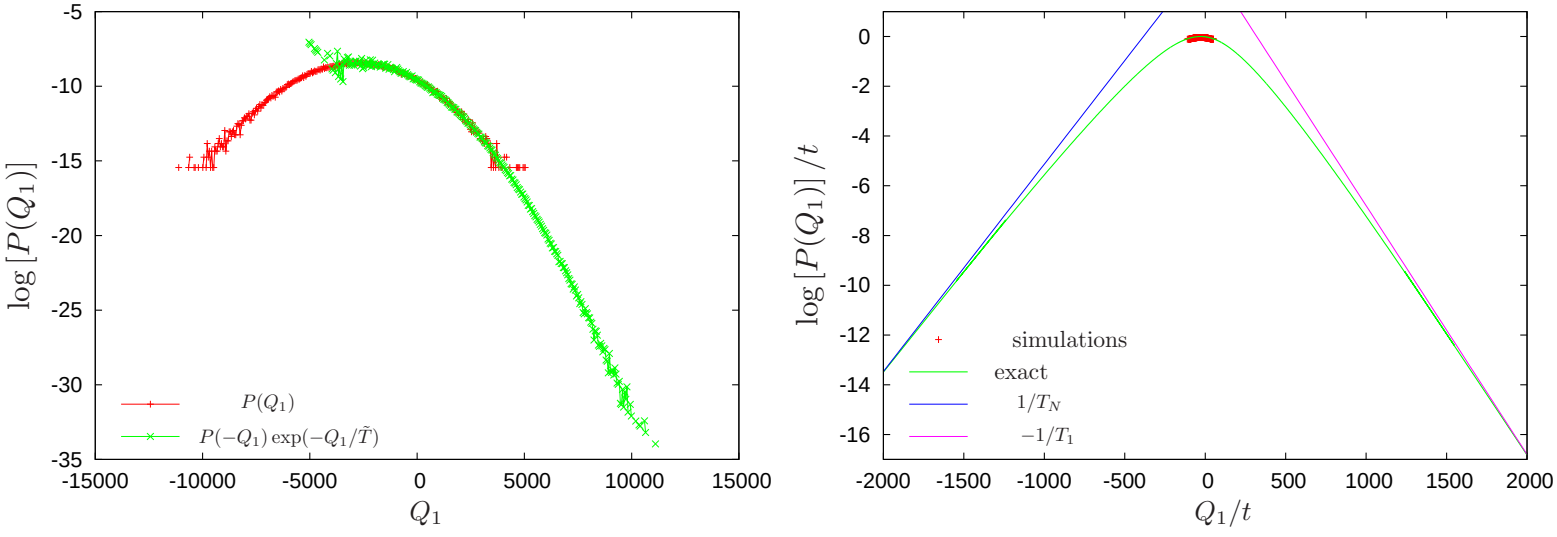

$t = 100$, $N = 10$, $T_1 = 100$, $T_N = 120$, 10^5 simulated trajectories, $\zeta = 10$, $k = 60$

H. Fogedby, AI, J. Stat. Mec. 2012;

H. Fogedby, AI, J. Stat. Mec 2014

An electric circuit with viscous coupling

S. Ciliberto, et al. PRL 2013

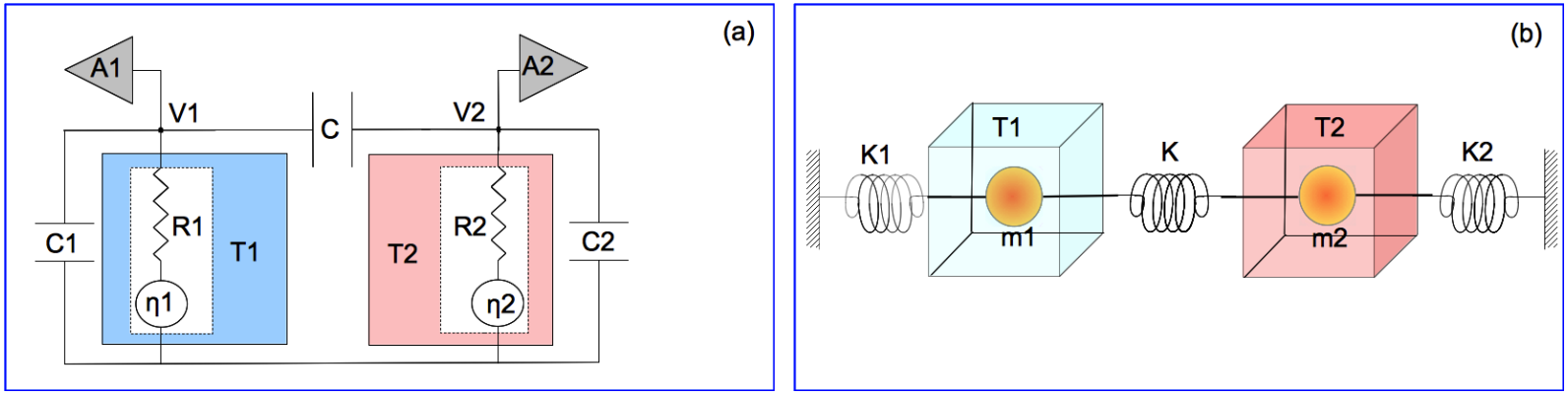

$$(C_1 + C)\dot{V}_1 = -\frac{V_1}{R_1} + C\dot{V}_2 + \eta_1$$

$$(C_2 + C)\dot{V}_2 = -\frac{V_2}{R_2} + C\dot{V}_1 + \eta_2$$

where η_i is the usual white noise: $\left\langle \eta_i \eta_j' \right\rangle = 2\delta_{ij} \frac{T_i}{R_i} \delta(t - t')$.

Nyquist effect

The potential difference across a dipole fluctuates because of the thermal noise

$$C\dot{V} = -\frac{V}{R} + \eta$$

$$\text{with } \left\langle \eta(t)\eta(t') \right\rangle = 2\frac{T}{R}\delta(t-t')$$

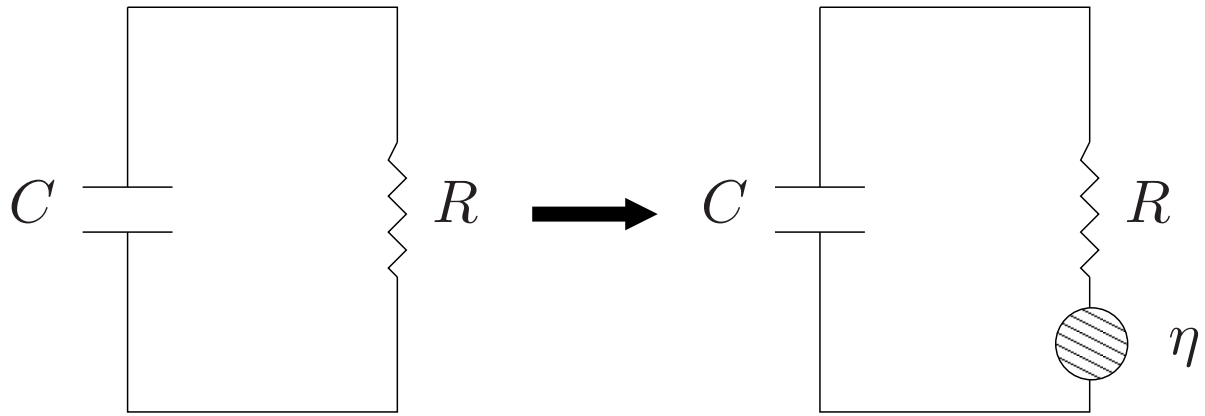

Thermodynamic quantities

- Dissipated power in an electric circuit

$$P = V \cdot I$$

- Heat dissipated in resistor 1

$$\begin{aligned} Q_1(t, \Delta t) &= \int_t^{t+\Delta t} \mathrm{d}t'\, C V_1(t') \frac{\mathrm{d}V_2}{\mathrm{d}t'} - (C_1 + C) V_1(t') \frac{\mathrm{d}V_1}{\mathrm{d}t'} \\ &= \int_t^{t+\Delta t} \mathrm{d}t'\, V_1(t') \left(\frac{V_1(t')}{R_1} - \eta_1(t') \right) \end{aligned}$$

- Analogous definition for Q_2

aka FT for Q_1 at $t \to \infty$: slow convergence

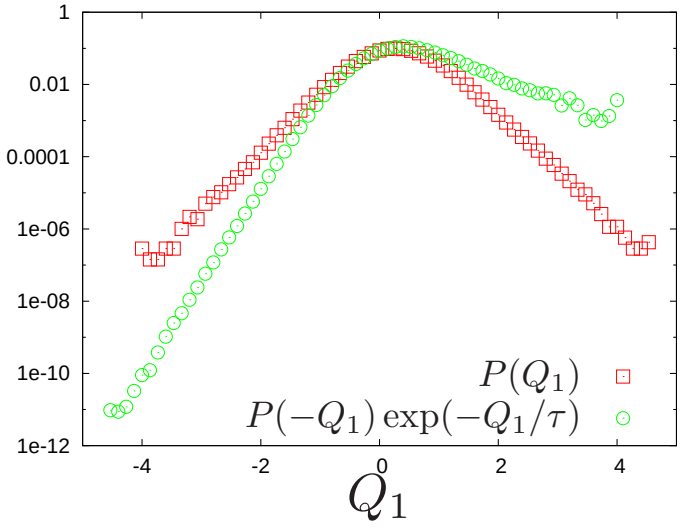

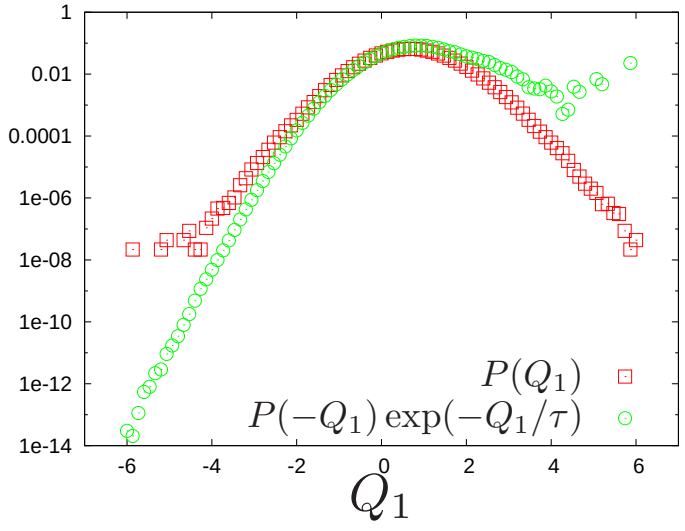

$\Delta t = 0.2$ s, $\Delta t = 0.5$ s

$$\log \frac{P_{\rm ss}(Q_1)}{P_{\rm ss}(-Q_1)} = -\tilde{\beta} Q_1$$

$\tilde{\beta} = 1/T_1 - 1/T_2$

$T_1 = 88$ K, $T_2 = 296$ K, $C = 100pF$, $C_1 = 680pF$, $C_2 = 420pF$ and $R_1 = R_2 = 10M\Omega$

A few definitions

- ΔS^{bath}: the entropy due to the heat exchanged with the reservoirs up to the time Δt

$$\Delta S^{\text{bath}}_{\Delta t} = Q_{1,\Delta t}/T_1 + Q_{2,\Delta t}/T_2$$

- the reservoir entropy $\Delta S^{\text{bath}}_{\Delta t}$ is not the only component of the total entropy production: entropy variation of the system?

A trajectory entropy

The system follows a stochastic trajectory through its phase space, the dynamical variables are the voltages $V_i(t)$.

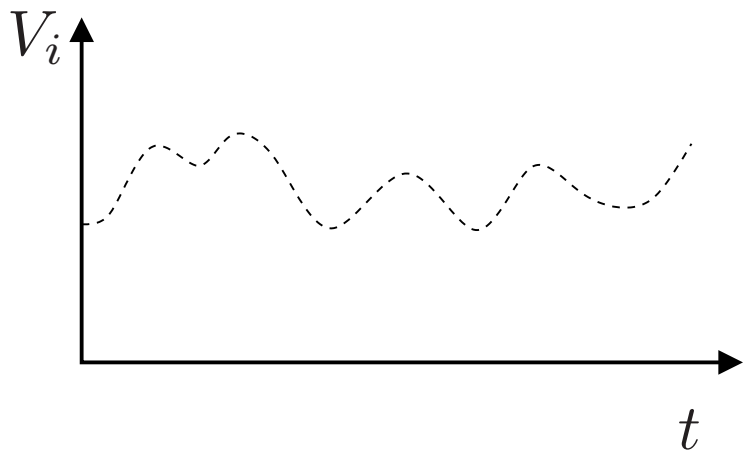

A trajectory entropy

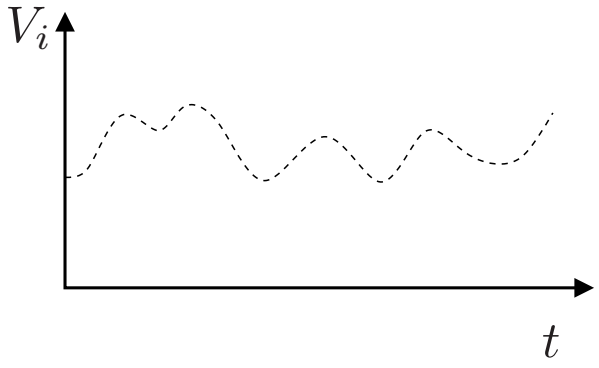

- Following *Seifert, PRL 2005*, for such a system we can define a time dependent trajectory entropy

$$S^{sys}(t) = -k_B \log P(V_1(t), V_2(t))$$

- Thus, the system entropy variation reads

$$\Delta S^{sys}_{\Delta t} = -k_B \log \left[\frac{P(V_1(t+\Delta t), V_2(t+\Delta t))}{P(V_1(t), V_2(t))} \right].$$

These are measurable quantities

- Q_i can be measured as discussed earlier
- $P(V_1, V_2)$ can be easily sampled

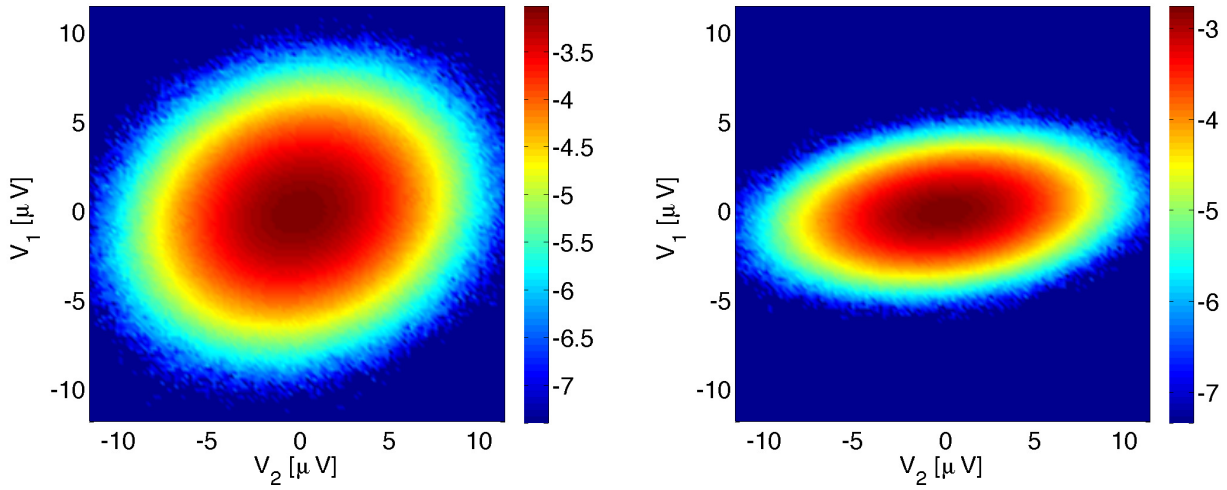

Left: $T_1 = 296$ K (eq.) right: $T_1 = 88$ K

- The system is in a steady state: $P(V_1, V_2)$ does not change with t

Total entropy

- Measure the voltages V_i at time $t = 0$ and $t = \Delta t$, and thus obtain

$$\Delta S^{sys}_{\Delta t} = -k_B \log \left[\frac{P(V_1(\Delta t), V_2(\Delta t))}{P(V_1(0), V_2(0))} \right].$$

- Measure the heats Q_1 and Q_2 flowing from/towards the reservoirs in the time interval $[0, \Delta t]$ and thus obtain

$$\Delta S^{\text{bath}}_{\Delta t} = Q_{1,\Delta t}/T_1 + Q_{2,\Delta t}/T_2$$

- Define the total entropy as

$$\Delta \mathcal{S}^{\text{tot}}_{\Delta t} = \Delta S^{\text{bath}}_{\Delta t} + \Delta S^{sys}_{\Delta t}$$

FT for the total entropy

- The theory predicts that the following equality holds

$$\left\langle \exp(-\Delta \mathcal{S}^{\mathrm{tot}}/k_B) \right\rangle = 1,$$

- We also know that the following FT holds for any trajectory $\boldsymbol{x}$

$$\widehat{\mathcal{P}}[\widehat{\boldsymbol{x}}] = \mathcal{P}[\boldsymbol{x}] \mathrm{e}^{-\Delta \mathcal{S}^{\mathrm{tot}}[\boldsymbol{x}]}$$

  which implies that $P(\Delta \mathcal{S}^{\mathrm{tot}})$ should satisfy a fluctuation theorem of the form

$$\log[P(\Delta \mathcal{S}^{\mathrm{tot}})/P(-\Delta \mathcal{S}^{\mathrm{tot}})] = \Delta \mathcal{S}^{\mathrm{tot}}/k_B, \;\; \forall \Delta t, \Delta T,$$

FT for the total entropy: experimental verification

$$\left\langle \mathrm{e}^{-\Delta \mathcal{S}^{\mathrm{tot}}/k_B} \right\rangle = 1, \quad Sym(\Delta \mathcal{S}^{\mathrm{tot}}) = \log\left[\frac{P(\Delta \mathcal{S}^{\mathrm{tot}})}{P(-\Delta \mathcal{S}^{\mathrm{tot}})}\right] = \frac{\Delta \mathcal{S}^{\mathrm{tot}}}{k_B}, \quad \forall \Delta t, \Delta T,$$

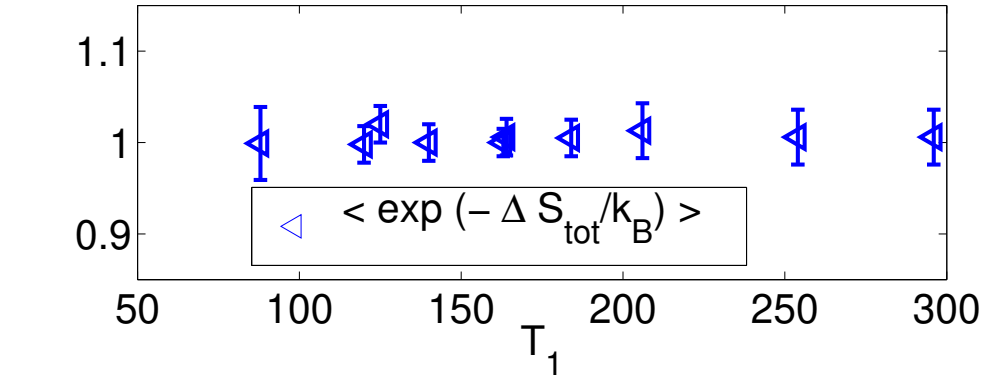

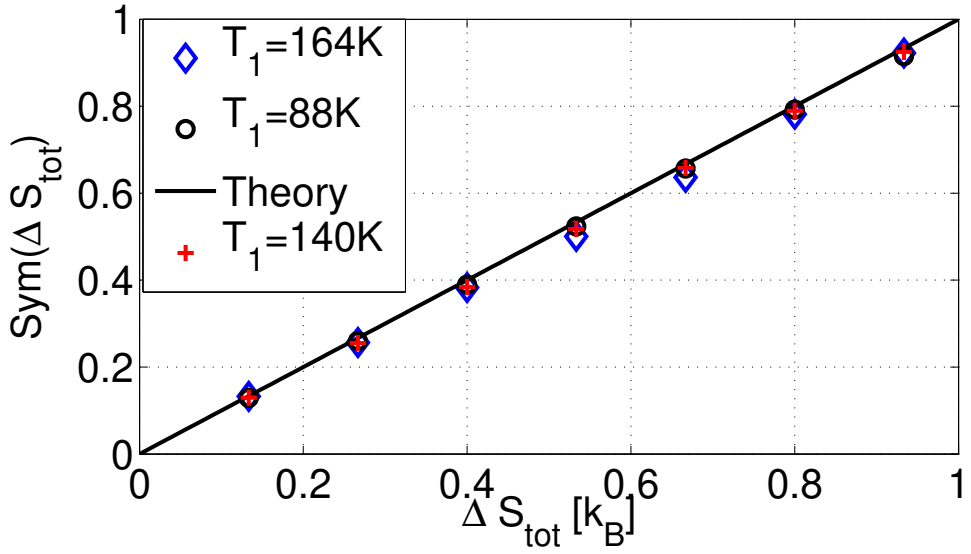

single-electron tunnelling events

nature physics

LETTERS

PUBLISHED ONLINE: 11 AUGUST 2013 | DOI: 10.1038/NPHYS2711

Distribution of entropy production in a single-electron box

J. V. Koski[1]*, T. Sagawa[2], O-P. Saira[1,3], Y. Yoon[1], A. Kutvonen[4], P. Solinas[1,4], M. Möttönen[1,5], T. Ala-Nissila[4,6] and J. P. Pekola[1]

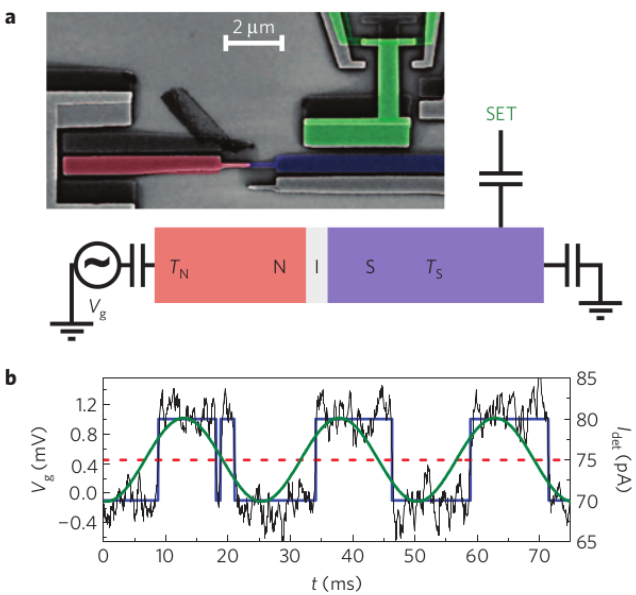

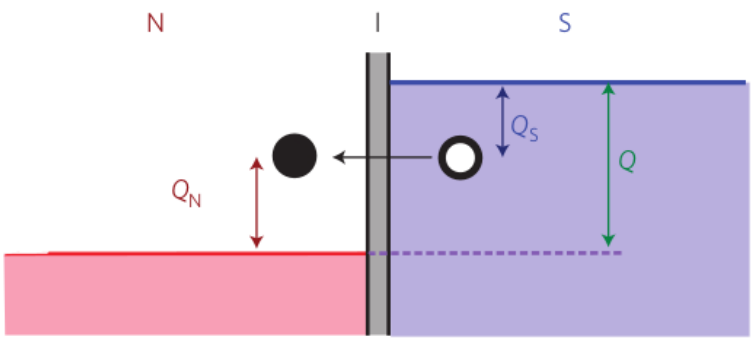

single-electron tunnelling events: FT

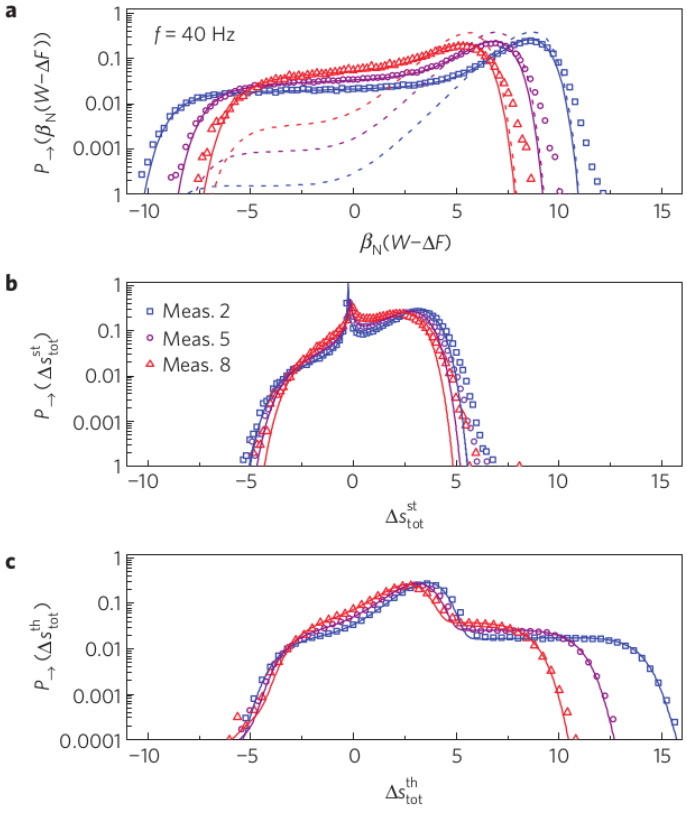

Figure 3 | Distributions of entropy production at different temperatures. **a**, $\beta_N(W-\Delta F)$ distributions for a 40 Hz forward protocol at different bath temperatures. The symbols show measured values (key in **b** applies to all panels), solid lines are numerical expectations (all panels), and dashed lines demonstrate what the distribution would be for $T_S = T_N$, such that Jarzynski Equality would be satisfied. **b**, Corresponding Δs^{st}_{tot} distributions. **c**, Δs^{th}_{tot} distributions for single jump trajectories.

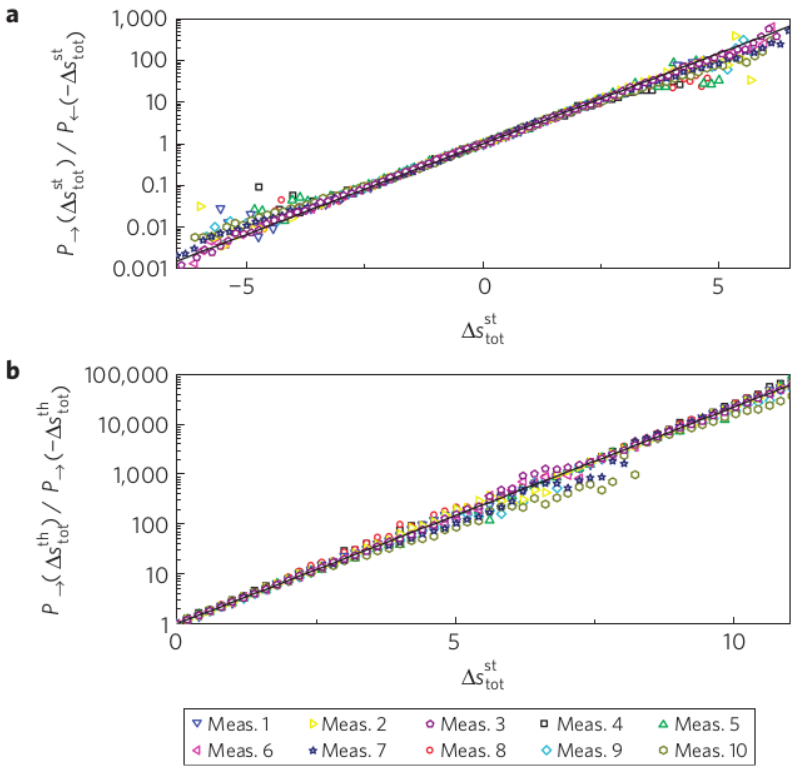

Figure 5 | Test of the DFR. a, DFR for Δs^{st}_{tot}. Despite the asymmetry of forward and backward protocols due to detector back-action, the relation is satisfied. **b**, DFR for Δs^{th}_{tot} of the forward protocol. In both **a** and **b**, the expected dependence given by equation (5) is shown as a solid black line.

Thermal cyclic engines: classical system

Realization of a micrometre-sized stochastic heat engine
Working fluid: a single colloidal particle in a laser trap

$$U(x,t) = \frac{k(t)}{2}x^2$$

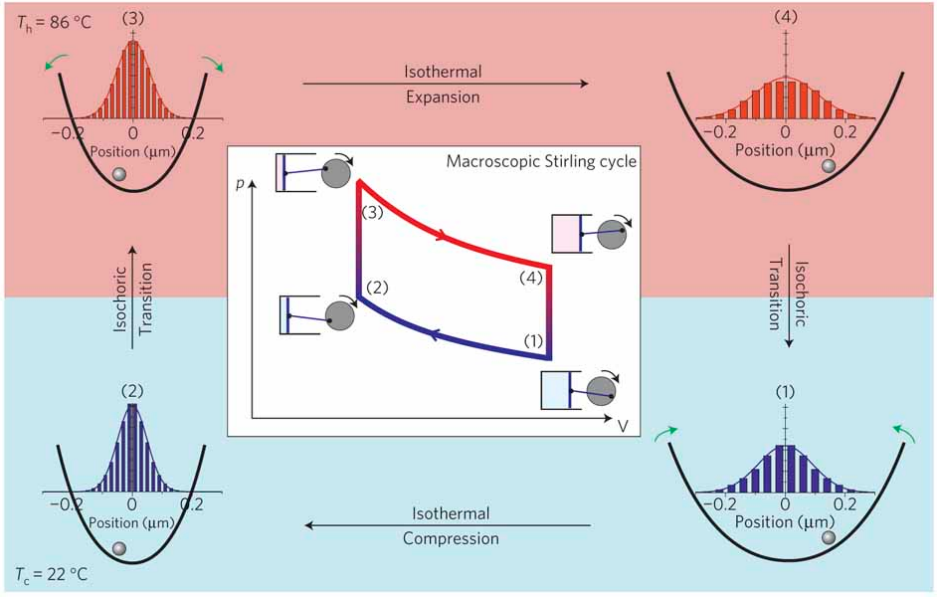

V. Blickle and C. Bechinger Nat Phys (2012)

Thermal cyclic engines: classical system II

NATURE PHYSICS DOI: 10.1038/NPHYS2163 LETTERS

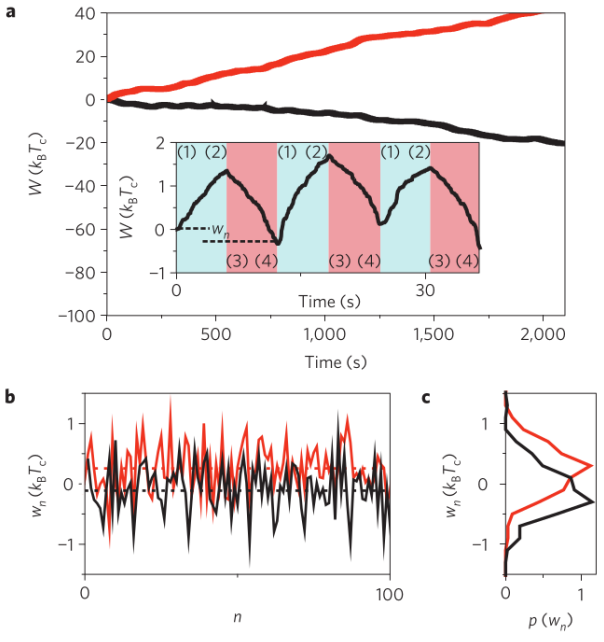

Figure 2 | Extracted work of the microscopic heat engine. a, W versus time for a heat engine in clockwise (black curve) and counter-clockwise (red curve) cycle direction with $\tau = 12$ s. In the latter case, the machine acts as a heat pump. (Inset) Magnified view where the individual steps during three cycles are resolved. **b**, Work accumulated over one cycle as a function of the cycle number n for clockwise (black) and counter-clockwise (red) cycle directions. The average work per cycle is $-0.11\,k_B T$ and $0.25\,k_B T$, respectively, for the two cases. **c**, Corresponding probability distributions, $p(w_n)$, to the plots in **b**.

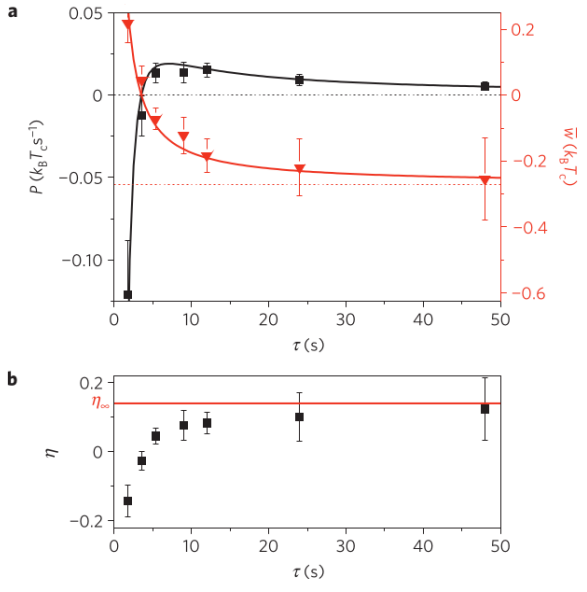

Figure 3 | Power, work and efficiency versus the cycle revolution time τ. **a**, Averaged work $\bar{w}$ and power as a function of the cycle time τ for the experimental conditions $T_h = 76\,^{\circ}\mathrm{C}$, $T_c = 22\,^{\circ}\mathrm{C}$, $k_{max}/k_{min} = 4.4$, $\bar{w}_\infty = -0.27\,k_B T_c$ and $\eta_c = 0.15$. The red solid line is a fit according to $\bar{w} = \bar{w}_\infty - \Sigma/\tau$ with the free fitting parameter $\Sigma = 0.95\,k_B T_c$s. For $\tau < 3.6$ s the machine is not extracting energy, $\bar{w}$ becomes positive and the output power negative. **b**, Efficiency η versus cycle time. In the long-time limit the measured efficiency approaches $\eta_\infty = 0.14$ (solid line). Note that the efficiency at maximum power is $\eta = 0.08$. The error bars indicate the standard deviations of the mean among individual cycles.

Motors and rotors of biological interests

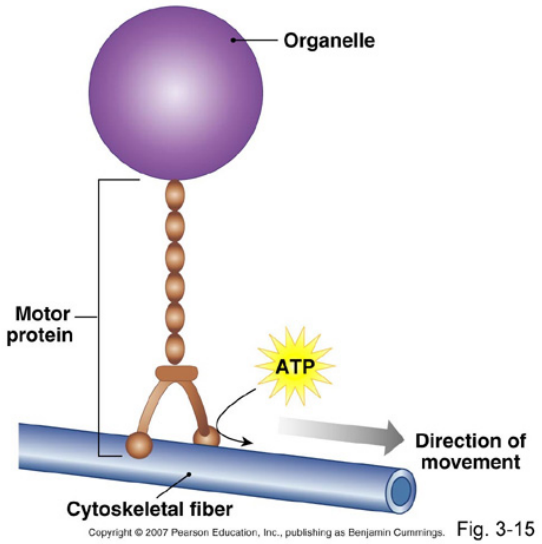

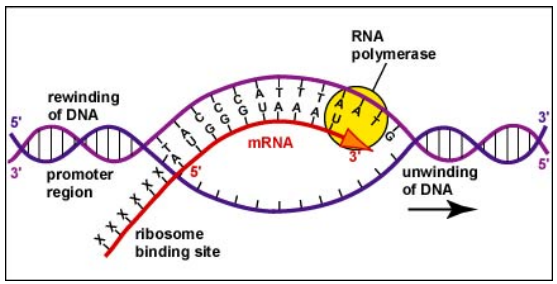

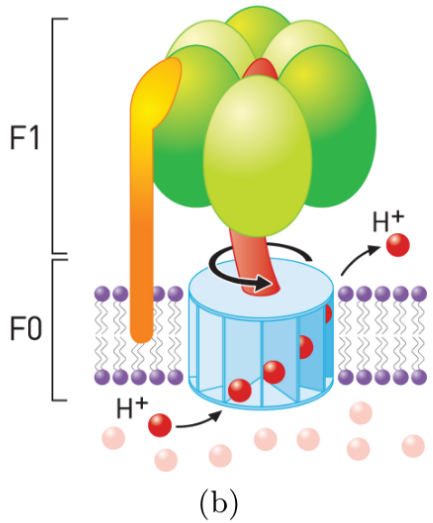

- Molecular motors are protein machines that convert chemical energy into useful work
- Example: Kinesin moves cargo inside cells along microtubules
- Example: RNA polymerase, transcribes DNA sequences into mRNA
- Example: ATP-synthase. The motor is driven by a proton gradient across the membrane.

Thermal cyclic engines: quantum system

A single-atom heat engine

Working fluid: a single calcium ion in a tapered ion trap

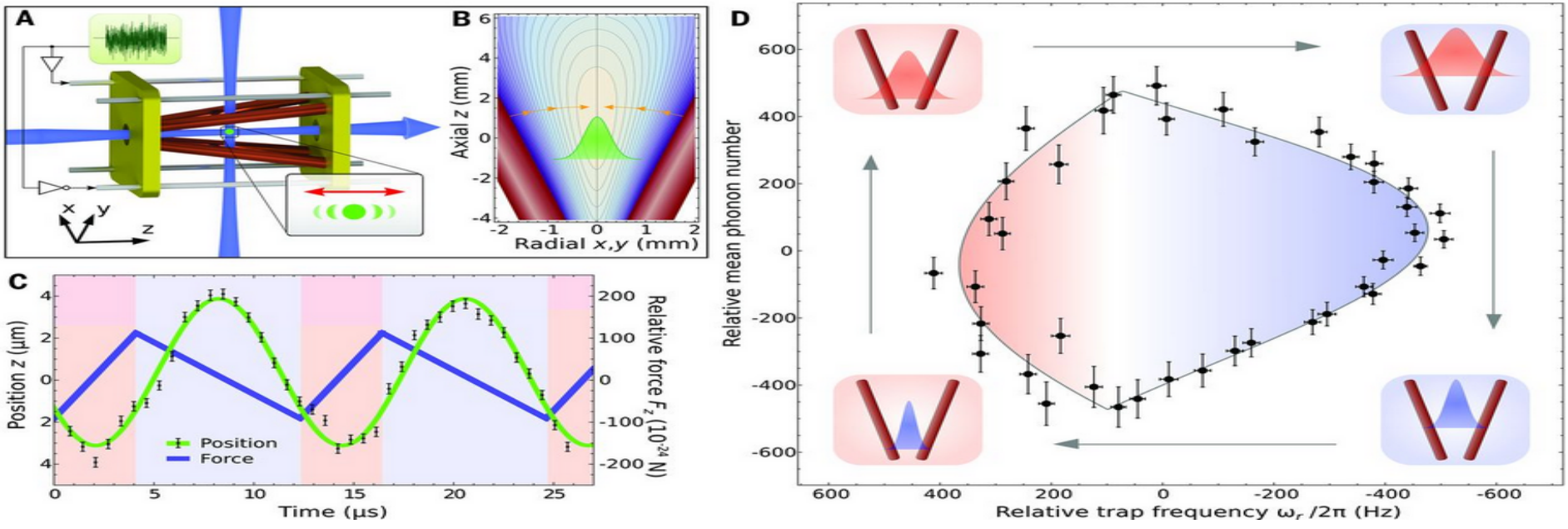

Johannes Roßnagel et al. Science (2016)

Quantum thermodynamics

Thermodynamics preceded quantum mechanics, and for many decades the two theories developed separately.
The gap is now being bridged

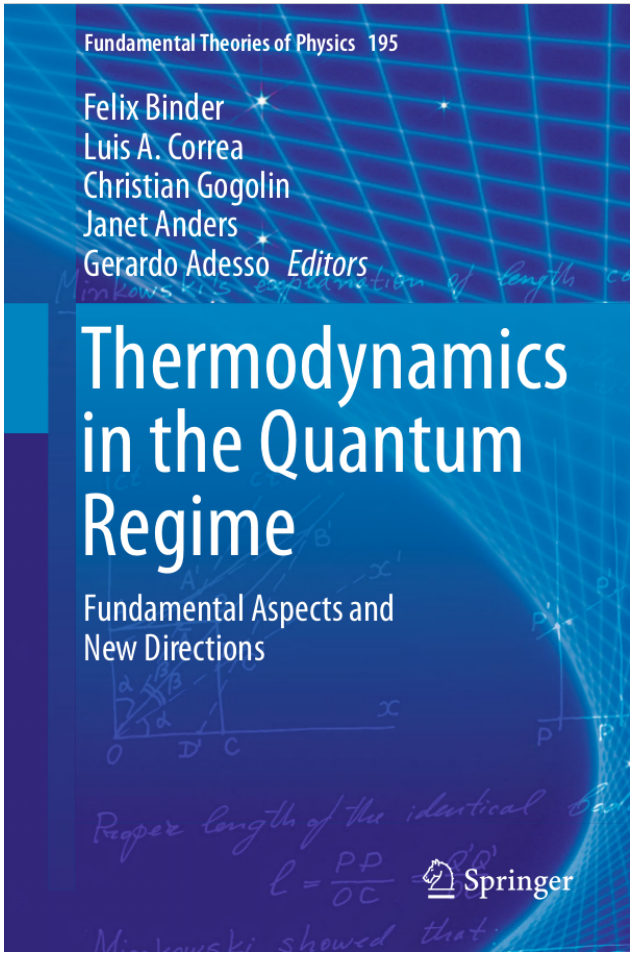

- How can process-dependent thermodynamic quantities, such as work and heat, be meaningfully defined and measured in quantum systems?
- What are the efficiencies of quantum engines and refrigerators? Are they better or worse than their classical counterparts?
- How do non-equilibrium fluctuation relations extend to the quantum regime?
- Which corrections to standard thermodynamic laws and relations have to be made when considering systems that couple strongly to their surroundings?

Quantum thermodynamics

Thermodynamics preceded quantum mechanics, and for many decades the two theories developed separately.
The gap is now being bridged

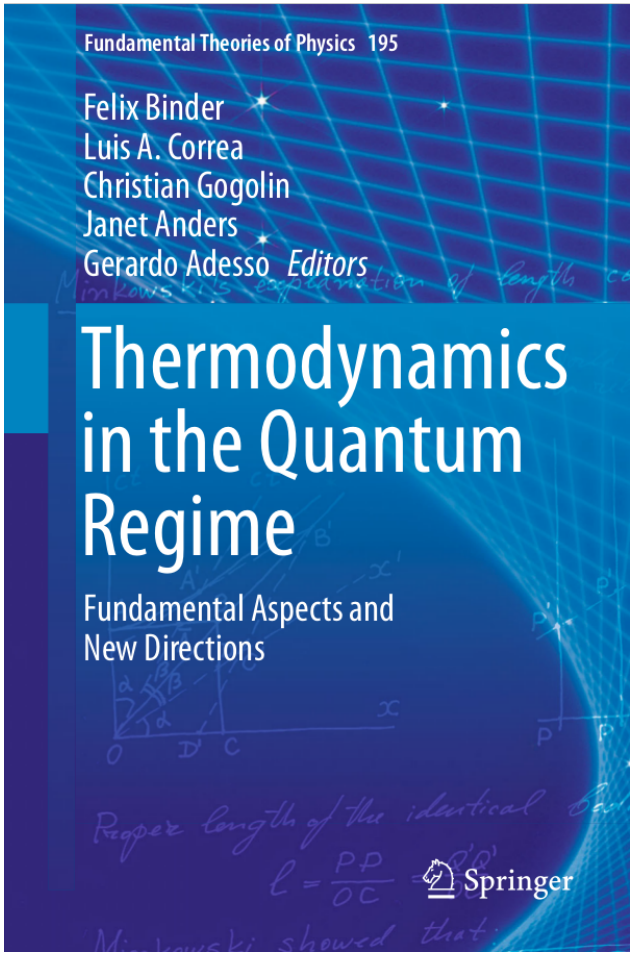

- How can process-dependent thermodynamic quantities, such as work and heat, be meaningfully defined and measured in quantum systems?
- What are the efficiencies of quantum engines and refrigerators? Are they better or worse than their classical counterparts?
- How do non-equilibrium fluctuation relations extend to the quantum regime?
- Which corrections to standard thermodynamic laws and relations have to be made when considering systems that couple strongly to their surroundings?

Thermodynamic of Information

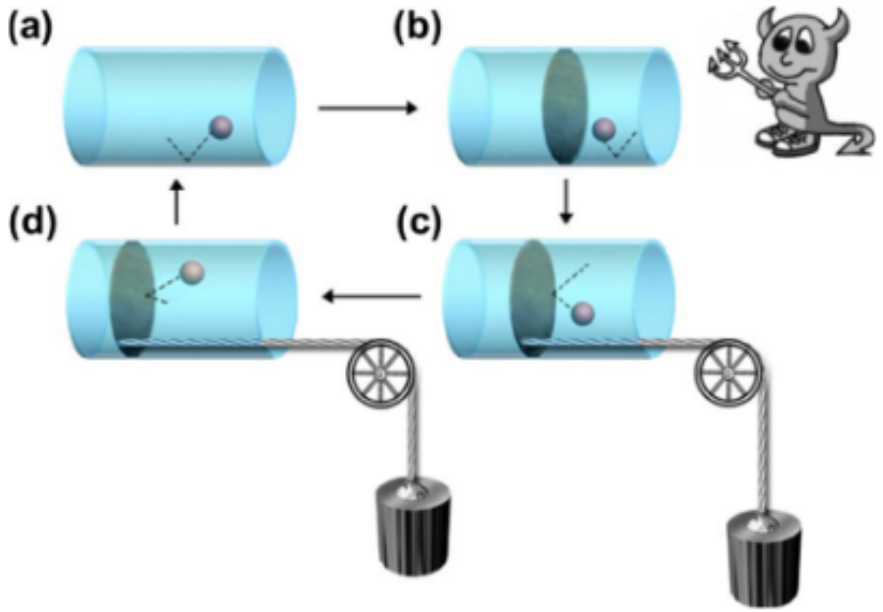

FIG. 1. (Color online) Schematic diagram of Szilard's heat engine. A chamber of volume V contains a one-molecule gas, which can be found in either the right or the left part of the box. (a) Initially, the position of the molecule is unknown. (b) Maxwell's demon inserts a partition at the center and observes the molecule to determine whether it is in the right- or the left-hand side of the partition. He records this information in his memory. (c) Depending on the outcome of the measurement (which is recorded in his memory), the demon connects a load to the partition. If the molecule is in the right part as shown, he connects the load to the right-hand side of the partition. (d) The isothermal expansion of the gas does work upon the load, whose amount is $kT \ln 2$ which we call 1 bit. Adapted from Fig. 4 in Plenio and Vitelli, 2001.

K. K. Maruyama, F. Nori, and V. Vedral
The physics of Maxwell's demon and information. Rev. Mod. Phys. 81, 1 (2009).

Landauer's principle

LETTER

doi:10.1038/nature10872

Experimental verification of Landauer's principle linking information and thermodynamics

Antoine Bérut[1], Artak Arakelyan[1], Artyom Petrosyan[1], Sergio Ciliberto[1], Raoul Dillenschneider[2] & Eric Lutz[3]†

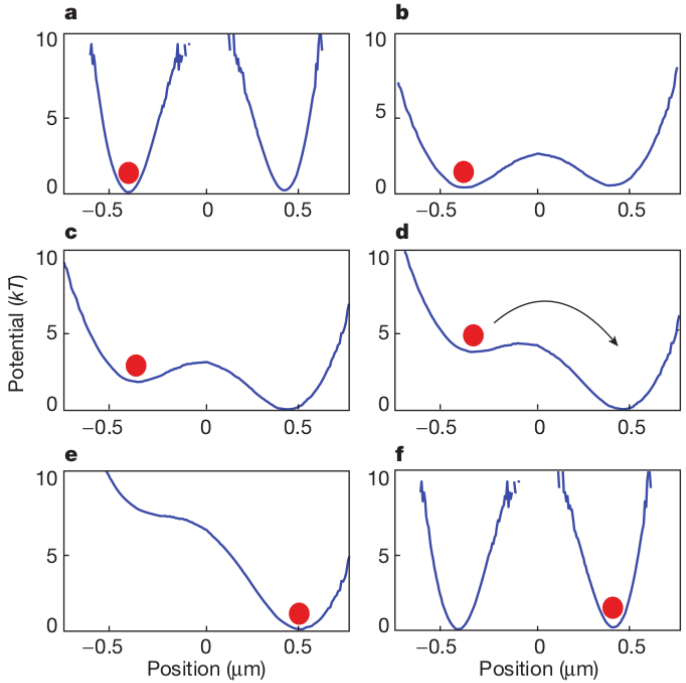

Figure 1 | The erasure protocol used in the experiment. One bit of information stored in a bistable potential is erased by first lowering the central barrier and then applying a tilting force. In the figures, we represent the transition from the initial state, 0 (left-hand well), to the final state, 1 (right-hand well). We do not show the obvious 1 → 1 transition. Indeed the procedure is such that irrespective of the initial state, the final state of the particle is always 1. The potential curves shown are those measured in our experiment (Methods).

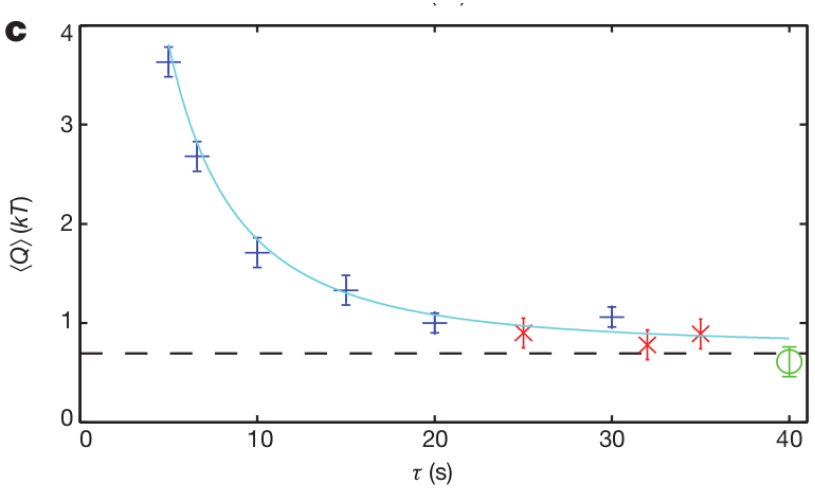

Information engine

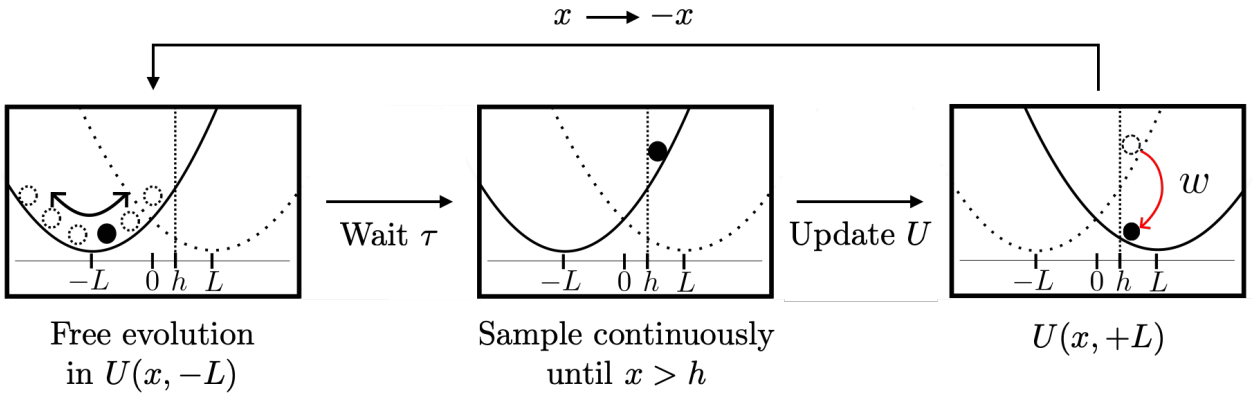

- Brownian particle in $U(x, \lambda) = k/2(x - \lambda)^2$, with $P(x, t = 0) = P^{eq}(x, \lambda = -L)$
- first passage at $x = h$
- extracted work $w = 2khL$

Tapes as information reservoirs

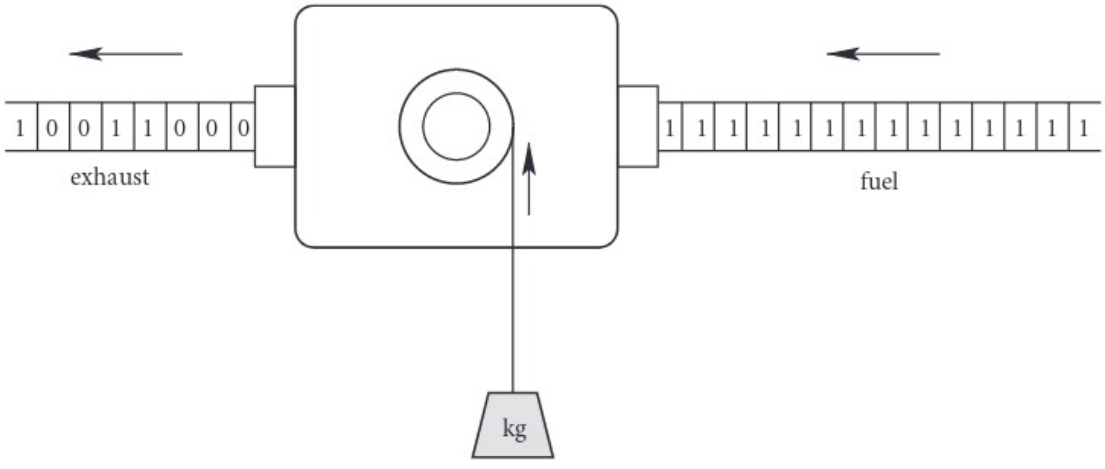

Figure 5.2. The Bennett-Feynman information-fueled engine. A tape (fuel) containing a large number of Szilard cylinders, each with the molecule in state 1 (right), is fed into the machine. Once inside, each cylinder undergoes the Szilard manipulation, and an average amount of work $-W = k_B T \ln 2$ is extracted. At the end of the manipulation, the location of the molecule in the cylinder is randomized (exhaust). See the discussion in Feynman [53, pp. 146–147].

from *PP, chapter 5*

Cooling of trapped atoms with a Maxwell's Demon

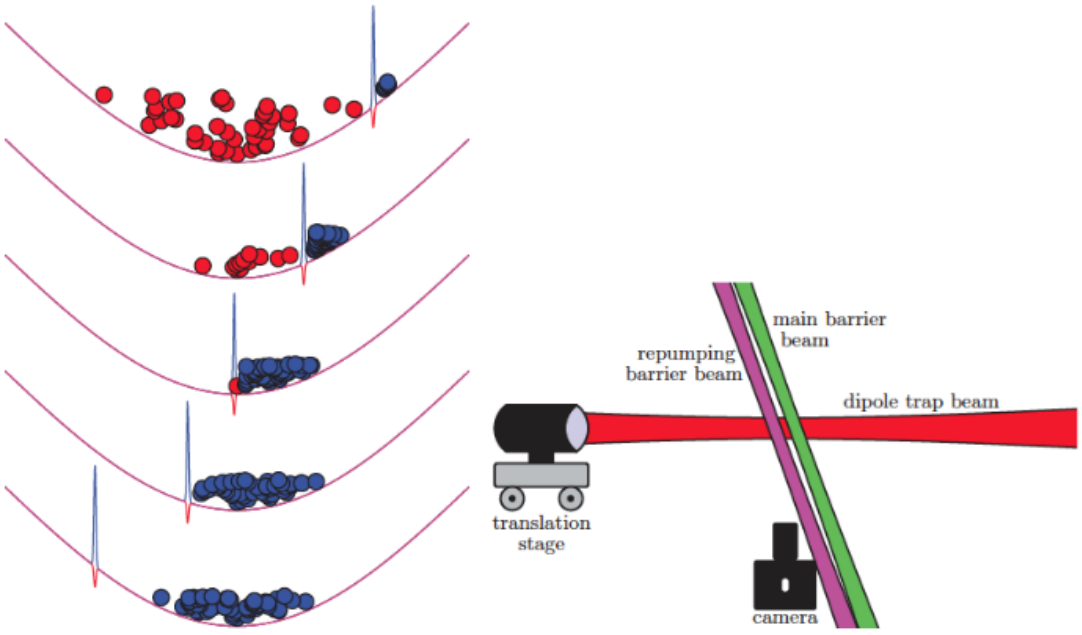

Figure 3: Using a Maxwell's demon to cool atoms. A pair of laser beams can be tuned to atomic transitions and configured to create a one-way potential barrier; atoms may cross unimpeded in one direction, from left to right left in this figure, but not in the other. Left panel : when the barrier is introduced at the periphery of the trapping potential, (right side) the atoms that cross the barrier will be those that have converted nearly all their kinetic energy to potential energy, in other words, the cold ones. By slowly sweeping the barrier (from the right to the left) across the trapping potential, one can sort cold atoms (blue) from hot ones (red), reminiscent of Maxwell's famous thought experiment, or cool an entire atomic ensemble. Because the cold atoms do work against the optical barrier as it moves, their kinetic energy remains small even as they return to the deep portion of the potential well. Right panel: schematic representation of the optical set-up showing the optical trap (red beam), the translational stage and the two beams one way barrier

Adapted from *M. G. Raizen, Science 324, 1403–1406 (2009)*

Climbing a staircase with a Maxwell's Demon

LETTERS
PUBLISHED ONLINE: 14 NOVEMBER 2010 | DOI: 10.1038/NPHYS1821
nature physics

Experimental demonstration of information-to-energy conversion and validation of the generalized Jarzynski equality

Shoichi Toyabe[1], Takahiro Sagawa[2], Masahito Ueda[2,3], Eiro Muneyuki[1]* and Masaki Sano[2]*

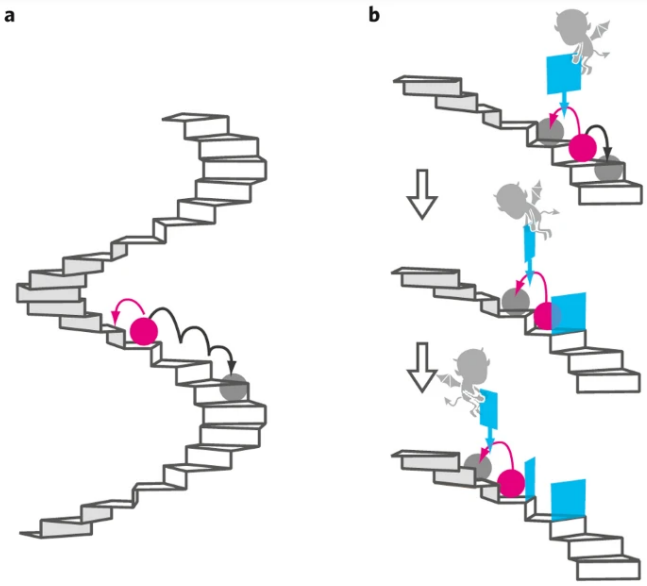

a, A microscopic particle on a spiral-staircase-like potential with a step height comparable to k_BT. The particle stochastically jumps between steps owing to thermal fluctuations. As the downward jumps along the gradient are more frequent than the upward ones, the particle falls down the stairs, on average. **b**, Feedback control. When an upward jump is observed, a block is placed behind the particle to prevent downward jumps. By repeating this cycle, the particle is expected to climb up the stairs without direct energy injection.

Figure 2: Experimental set-up[29,30].